"REVIEWED"

A PRELIMINARY APPRAISAL OF THE NATURAL STRUCTURE AND SEEDABILITY OF UPDRAFTS IN MIDWESTERN CUMULUS AT THE -10°C LEVEL

Robert R. Czys
Illinois State Water Survey
Atmospheric Sciences Division
Office for Cloud and Precipitation Research
Champaign, Illinois 61820

ABSTRACT. The properties of 40 updrafts in 11 warm-based Midwestern cumulus congestus are characterized on the basis of aircraft data collected at the -10°C level during the 1986 Precipitation Augmentation for Crops Experiment field program. Typically, clouds in this sample were found to be composed of multiple updrafts, with one updraft encountered on average for every 1.5 km of cloud penetrated. Mean updraft velocities ranged from 1 to 12 m s^{-1}, with a sample average of 4.2 m s^{-1}.

All updrafts contained at least some supercooled liquid water content in the size range of cloud droplets ($D < 50$ μm). Cloud droplet liquid water content was low, typically 0.3 g m^{-3}, and bimodal cloud droplet size distributions were occasionally observed. Most updrafts contained supercooled drizzle and raindrops. The mass of supercooled drizzle and raindrops was often as large or larger then the mass of supercooled cloud droplets, indicating an efficient coalescence process.

Sub-millimeter-size graupel was the apparent dominant first ice form, often occurring in concentrations that exceeded those conventionally expected from ice nuclei by factors from 10 to 100. Images of vapor-grown ice crystals were not often identified in the records from 2D optical array probes. Thus it is likely that the very first ice initiated from the freezing of supercooled drizzle and raindrops. Aircraft instrumentation available to the 1986 field program was not adequate to detect ice smaller than approximately 150 μm diameter. Secondary ice production (SIP) by Hallett-Mossop rime-splintering could not be verified on the basis of available information.

Natural updraft buoyancies were often close to neutral, and the amount of loading by the condensate was found to have deciding influence on net buoyancy. The results of calculations suggest that buoyancy enhancements are feasible by seeding, particularly for clouds with substantial water loads and moderate updrafts. However, discerning seeding effects will be complicated by large variations in initial conditions for seeding.

1. INTRODUCTION

The mixed-phased properties of natural cumuli are being studied as part of the Precipitation Augmentation for Crops Experiment (PACE). PACE is an interdisciplinary research program designed to determine the precipitation alterations possible by seeding to achieve a dynamic response in cloud behavior, as well as the benefits and liabilities associated with precipitation augmentation. The overall goals and objectives of PACE have been discussed by Changnon (1986). The exploratory-seeding phase of PACE began in the summer of 1986 with a field program (coined PACE86) using Doppler radar, instrumented aircraft, and a state-of-the-art forecasting/nowcasting system. The aircraft data presented in this paper are unique in that they form the first extensive set of modern cloud physics measurements taken at the -10°C seeding level within the type of youthful, moderately vigorous, warm-based cumulus thought to be ideal candidates for dynamic seeding (Woodley, 1970).

Observational study of the dynamical and physical nature of Midwestern summertime convection has a long history; a comprehensive survey has been provided by Ackerman and Westcott (1986). The Thunderstorm Project (Byers and Braham, 1949) pioneered the use of aircraft and radar to investigate cloud dynamics in the Midwest. However, no microphysical measurements were made during this study because suitable instrumentation was not available. Microphysical data collected as part of Project Whitetop (Braham, 1964) are probably the most comparable to those collected in PACE86, and great similarity can be found between precipitation processes reflected in Whitetop and PACE86 microphysical data.

Other modern microphysical measurements in mixed-phased regions of Midwestern clouds have been taken as a part of the planning phase of PACE. In 1978, with the support of NOAA scientists, the P-3 aircraft was used and obtained a sample of microphysical data mostly around the melting level, but

the weather situations were more typical of spring than of summer (Ackerman *et al.*, 1978). In 1980, with the aid of the University of Wyoming King Air, data were collected that pertained primarily to the melting level of convective elements embedded in stratiform clouds. The properties of the updrafts of these clouds have been reported on by Politovich and Reinking (1987). Hence, even though the sample of PACE86 clouds is not as large as desirable and the extent to which these findings generally apply to other summers is uncertain, these data add considerably to the information about the nature of mixed-phased conditions at the -10°C seeding level in Midwestern summer convective clouds and the implications for seeding.

2. AIRCRAFT, INSTRUMENTATION AND DATA REDUCTION

A light, turbocharged, twin-engine airplane (a Beechcraft Baron) was used to collect the data. The airplane has a service ceiling of about 7 km (≈23 kft), a typical rate of climb of 3.5 m s^{-1} (≈700 ft min^{-1}), and a cruising true airspeed between 80 and 100 m s^{-1}. The airplane was equipped with a full range of particle spectrometer and particle measuring systems (PMS) optical probes (FSSP, 2DC-OAP, and 2DP-OAP), a Johnson-Williams (JW) hot-wire probe for measuring cloud droplet liquid water content, and instrumentation for measuring thermodynamic parameters such as temperature, pressure, and dew point. A forward-looking video camera was used to record the condition of the sky outside of cloud, to record the condition of the airplane windshield when inside cloud (which was useful in verifying 2D indications of cloud regions with high and low supercooled water content), and to make a verbal record of mission experiences.

Vertical air velocity was estimated by using a method discussed by Lawson (1979): vertical air motions are determined from knowledge of the atmospheric motion with respect to the airplane and the airplane's motion with respect to the earth. These motions are either measured directly or determined from measurements of true air speed, vertical motion, angle of attack, and pitch angle. The calculation includes compensation for angular acceleration around the airplane's lateral axis. The method works best when the airplane flies straight and at constant pitch and then is allowed to "float" with the vertical motions imposed by the cloud. This method is at its worst if the aircraft experiences either rapid pitch movements or excessive bank angles. Work by Lenchow (1976) has suggested that inertial effects which would produce response lags are tolerable if a lightweight aircraft such as the Baron is used. Thus, this error has not been corrected for in the vertical air motion data, otherwise estimated to be within about ±0.5 m s^{-1} of the presented values.

Quantification of the 2DP and 2DC image records was accomplished by using interactive software developed in-house for PACE86 data. The quantification procedure began by manual classification of image types on a paper copy of the image record for each penetration (i.e., those images that might be drops, graupel, ice crystals, crystal fragments, or aggregates were labeled). Images which were likely artifacts were not labeled. Once the images were labeled, an interactive program was run to digitize the image data.

Classification of artifacts and simple diode configurations such as zero-area images, one-diode images, twin-diode images, streakers, and streamers occurred automatically as the program scanned through the image records (see Heymsfield and Baumgardner, 1985, for 2D probe terminology). Information about these image types was retained in the classification data set for later use if needed. Manual entering of a character code was required when more complicated geometric configurations were encountered.

In general, the computer program primarily displayed large circular images since the presence of hexagonal ice forms in the 2D record was extremely rare. For example, for an "entire-in" image to be considered, it had to be at least 6 diodes large measured parallel and perpendicular to the time slice to have enough information to resolve particle shape and roughness. Thus, using the labeled paper copy of the images as guidance, the program operator had to make a final visual judgment on the smoothness of the image and thus discriminate images that were probably created by drops from those that were probably created by graupel. In the process of tagging images, the program maintained an accounting of the timing marks for subsequent use in calculating sample volume.

There are several sources of measurement uncertainty associated with image processing that must be taken into account when viewing values derived from the 2D data. First, all whole images showing smooth circular symmetry were counted as liquid drops even though they may have been frozen. Thus, an inability to distinguish between liquid and frozen drops has probably led to an overestimation in amounts for supercooled drizzle and raindrops. Playback of the forward-looking videotape clearly shows splashing on the windshield during certain portions of cloud penetrations. Hence the classification of smooth circular images as supercooled raindrops is usually supported by visual evidence recorded on videotape.

Another source of error is associated with the resolution of probes (approximately 25 μm for the 2DC and 200 μm for the 2DP). Thus, for any fairly circular image, it is easier to identify roughness in the 2DC records then in the 2DP records because smaller irregularities can be resolved in the former. Therefore, some additional errors associated with judging the roughness of an image cannot be ruled out. This error in judgment has probably resulted in a bias toward smooth images, particularly in the 2DP records.

A very important source of measurement uncertainty is associated with the extremely small cloud volumes sampled by the 2D probe. Sample volumes are especially small because data are limited to observations in updraft regions. On the basis of the Poisson statistics discussed by Cornford (1967), it is estimated that approximately 70% of the 2D concentrations for drops and graupel presented here are on average within 50% of the "true" value. However, because no method exists to quantify the other sources of errors, no precise statement can be made at this time about the measurement uncertainties regarding values derived from the 2D data.

3. CONVECTIVE ENVIRONMENT

3.1 Conditions on 8 July 1986

On 8 July 1986, seven different cumulus congestus were sampled feeding an air-mass

thunderstorm that originated to the west-southwest of Indianapolis, Indiana, USA. The synoptic-scale weather pattern on this date was dominated by a stationary front running westward from New York State through the Great Lakes region and into west-central Iowa. About the time that microphysical observations were being taken, the surface weather south of the front was characterized by light south-westerly winds converging within a moist region 70 km wide, centered on a line extending from South Bend, Indiana, to Vincennes, Indiana. Highs in the area were reaching above 32°C (90°F) and dew points were around 22°C (72°F).

Convective activity was triggered by weak advection of positive vorticity into the region co-incident with the time of maximum heating. A CLASS (Cross-chain Loran Atmospheric Sounding System supplied by the National Center for Atmospheric Research, NCAR) sounding (see Fig. 1) taken a few hours earlier at Champaign, Illinois (CMI) showed a neutrally stable atmosphere from the surface to the convective condensation level (CCL @ 1.7 km and 16°C or 5.5 kft and 61°F), which agrees closely with airborne estimation of cloud-base height and temperature. Above the CCL, conditionally unstable air existed to about 9.1 km (30 kft). The height of the melting level was 4.4 km (14.5 kft), and the depth of the -3 to -8°C layer was about 0.9 km (3 kft). The atmosphere gradually moistened from the surface to 900 mb and then dried out again through a 200 mb deep layer up to 450 mb. As can be seen in Fig. 1, no shallow inversion at mid-tropospheric level existed to limit the vertical growth of the clouds. The National Weather Service (NWS) radar summary for 2035 UT indicated that maximum echo tops were reaching 16.8 km (55 kft) for the larger storm clouds in the vicinity of sampling, consistent with what might be diagnosed from the NCAR/CLASS sounding (the Indianapolis metropolitan area was out of the range of the then Champaign, Illinois based CHILL radar).

The clouds sampled on 8 July were associated with storms that eventually produced damaging winds,

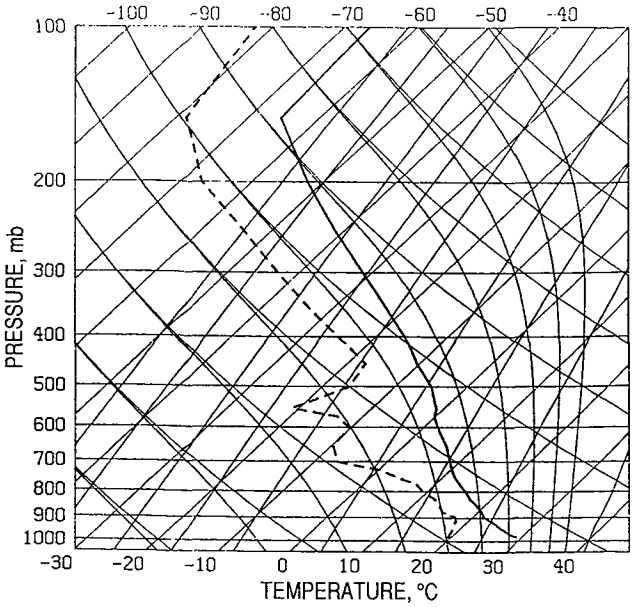

Figure 1. NCAR/CLASS sounding released from CMI at 1649 (LT) on 8 July 1986.

locally heavy rainfall and hail. At 1913 UT the National Severe Storms Forecast Center issued a severe thunderstorm watch for parts of eastern Illinois and much of northern Indiana, and by 1950 UT the NWS weather service in Indianapolis reported tree damage on the western side of Indianapolis. At 2025 UT, a gust of ≈30 m s^{-1} (70 mph) was reported at Indianapolis Power and Light, just 16 km (≈10 miles) southeast of the airport. At 2110 UT, 1.3 cm (half-inch) diameter hail was reported hitting Danville, Indiana, which is located just 24 km (≈15 miles) east of Indianapolis. By 2225 UT the storms had moved immediately east of Indianapolis into northern Shelby and southern Hancock counties.

3.2 Conditions on 24 July 1986

Data are available for four isolated cumulus congestus that were sampled in north central Missouri on 24 July 1986 . This system occupied a generally larger horizontal area and was less fragmented than the storms that occurred on 8 July, thus reflecting stronger, better organized synoptic-scale forcing. At the surface, a complex pattern of cold and warm fronts was connected to areas of cyclonic circulation; one centered in central Ontario, Canada, and the other centered on the South Dakota/Nebraska state border. Weak south-southeasterly cross-isobaric flow occurred over the region east of the fronts throughout much of the day. As on 8 July, surface temperatures reached into the mid-90s (≈35°C) and dew points into the 70s (≈21°C). On 24 July, an 850 mb trough was present with axis centered along the surface frontal system extending into Canada. A large area of positive vorticity was positioned at 500 mb over almost all of north-central Missouri and was forecast to move slowly to the northeast with diminishing intensity.

Cloud base temperature and height estimated during the mission were 15°C and 2.0 km (or 59°F and 6.6 kft), respectively. A representative vertical profile of temperature and humidity is not available because of poor radiosonde coverage in this part of the Midwestern USA. However, a sounding constructed from the aircraft data gave no indication of a mid-level limit to the vertical growth of the convection. In the NWS radar summary issued for the time of sampling, maximum echo tops were reaching 12.2 km (≈40 kft). Unlike the storms on 8 July, convective activity initiated in the early morning and persisted throughout most of the early afternoon, dissipating well before sunset.

4. OPERATIONAL PROCEDURES

Cloud selection was made by the flight meteorologist in collaboration with the pilot according to visual criteria set forth in the PACE86 Operations Manual. Missions were planned around penetrating clouds which were either just reaching or vigorously passing through the -10°C isotherm (≈6.1 km or 20 kft over Illinois in the summer). Clouds were to show (a) an appearance indicating continued vertical growth, (b) a sharply defined outline, like that of a cauliflower, (c) a substantial horizontal dimension (i.e., the cloud should be stout rather than tall and thin), and (d) a limited vertical slope, if any. The data presented in this paper are for clouds which met all these criteria.

The Operations Manual specified that near-direct central penetrations be made whenever safety

permitted; such is the case for the data presented herein. Detection of cloud droplets by the FSSP was used to define cloud edges. Thus, cloud and updraft sizes are representative of diameters calculated by multiplying the mean true airplane speed by the time spent either in-cloud or in-updraft, respectively.

With the assistance of the pilot, cloud maturity was approximated on approach to each cloud from a visual estimation of the amount of cloud above flight level. The maturity of the clouds presented in this paper can be placed in two broad categories: "young" clouds, those with tops greater than 0.15 km (≈500 ft) but less than 0.8 km (≈2.5 kft) above the level of initial penetration; and "older" clouds, those with tops between 0.8 and 1.5 km (2.5 and 5.0 kft) above the initial level of sampling. Cloud-top temperatures have been estimated on the assumption of a moist adiabatic lapse rate of -2°C per 305 m (or -2°C/1.0 kft) and fall in the range from approximately -11 to -15°C for "young" clouds and approximately -15 to -20°C for "older" clouds.

5. DATA

5.1 Cloud kinematics

An updraft was defined as any region in-cloud where vertical winds were estimated to be greater than 1 m s^{-1} for at least 3 continuous seconds of flight. Thus, by limiting the minimum updraft dimension to approximately 250 m, the results of adiabatic and collection processes occurring within the framework of larger-scale dynamic forcing are dominantly represented. However, the effects of turbulent dilution are not precluded, as will become evident.

In the total of 11 clouds, 40 distinct updrafts were identified: 28 in the 8 young clouds, and 12 in the 3 older clouds. Some general geometric properties of the clouds and updrafts are summarized in Table 1. Listed are the cloud identification in the form of month, day, cloud number, and penetration number. Cloud maturities are indicated as either young (**) or older (****). Table 1 also lists the air temperature prior to penetration (°C), cloud diameter (m), number of updrafts per cloud, the percent of cloud with updraft, and the frequency of updraft occurrence for each kilometer of cloud diameter. The plus sign following the number of updrafts in cloud 724c8p1 (July 24, cloud 8, penetration 1) indicates that data were recorded for only the first portion of the penetration as a result of a data system failure. Restricting the analysis to updrafts larger than 300 m would have reduced the number of updrafts by 2 in the young sample and by an additional 2 in the older cloud sample. Further restricting the analysis to 500 m minimum lengths additionally reduces the number of updrafts for analysis by 6 and 1 for young and older clouds, respectively.

As can be inferred from Table 1, although the clouds were observed during the very early part of their lifetimes, they were not composed entirely of one extensive updraft, but rather of several distinct regions of rising air surrounded by regions of falling air. The number of updrafts per cloud ranged from 2 to 5, with most clouds composed of either 3 or 4. As is evident in Table 1, larger clouds contained more updrafts than smaller clouds. The general rule of thumb for this sample is to expect at least 1 updraft for each 1.5 km diameter of cloud.

Table 1. Summary of Cloud and Updrafts Properties.

ID	Maturity	Tp °C	Diameter km	No. per cloud	%Cloud w/updraft	Frequency km^{-1}
708c1p1	**	-8.6	0.4	3	60	1.3
708c3p1	****	-9.3	0.9	5	74	1.7
708c5p1	**	-8.9	0.8	5	85	1.6
708c7p1	**	-10.6	0.6	4	69	1.6
708c11p1	**	-9.7	0.5	4	68	1.3
708c12p1	**	-8.4	0.4	3	68	1.3
708c14p1	**	-8.8	0.5	3	58	1.8
724c1p1	****	-9.3	1.0	4	67	2.5
724c5p1	**	-8.1	0.4	4	31	1.1
724c7p1	****	-7.7	0.6	3	28	2.1
724c8p1	**	-8.1	0.4	2+	23	1.9

The distribution of mean velocities for the 28 young-cloud updrafts is shown in Fig. 2. Bimodality is evident in this sample, with a major peak falling in the 1 to 3 m s^{-1} category and a secondary maximum occurring in the 5 to 6 m s^{-1} category. This bimodality reflects the multiple updraft structure of the clouds. As can be seen, mean updraft velocities ranged from 1 to 12 m s^{-1} with a sample average of 4.2 m s^{-1}. Thus, on average the fall speed of drops about 800 μm in diameter would typically tend to balance with the updraft velocity.

Each cloud in the young-cloud population had a main or largest updraft. However, the largest updraft geometrically was not necessarily the one with the strongest velocity. The average size of the main updraft was approximately 1350 m, with some as small as 450 m and others as large as 3000 m. Four of the eight main updrafts had the biggest peak velocity. In two cases, the clouds were composed of multiple strong updrafts (10 to 15 m s^{-1}) which were within 200 or 300 m of one another. Of the remaining clouds, two were composed of multiple weak updrafts (1.5 to 2.5 m s^{-1}) within 300 m of each other.

5.2 Supercooled cloud droplets

Cloud droplets are important to precipitation initiation and growth. Being easily evaporated, they also compensate the vapor field for losses due to entrainment. At temperatures colder than 0°C,

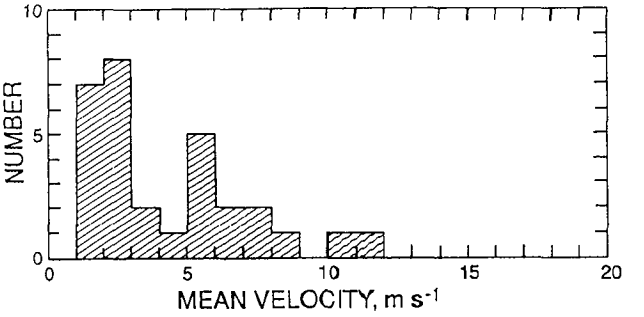

Figure 2. Distribution of mean updraft velocities in young clouds.

cloud droplets are the main supply for ice crystal growth by deposition. They are also the main substance for accretion growth of graupel, and supercooled drizzle and rain drops. Furthermore, the relative presence or absence of certain sizes of cloud droplets can positively or negatively influence the rate of secondary glaciation processes, such as rime-splintering (Hallett and Mossop, 1974).

Table 2 summarizes characteristics of the cloud droplet population as indicated by measurements taken with the JW and FSSP probes for each cloud (C_ID) and updraft (U_ID) in the PACE86 sample. An asterisk indicates the main updraft of each cloud. Listed for each updraft are the peak and mean value of cloud liquid water content as indicated by JW (labeled as PJWC and MJWC, respectively) or as calculated from FSSP data (labeled as PFWC and MFWC, respectively). FSSP measurement of cloud droplet mean diameter (DBAR) is given in units of μm, and mean (MCONC) and peak concentrations (PCONC) are in units cm^{-3}.

Obtaining a good measure of the character of the cloud droplet population, particularly in mixed-phase conditions, is difficult. For example, artificial broadening of the size spectrum has been noted as well as other limitations of the FSSP related to electronic response, optical resolution, and calibration uncertainties (e.g., Cerni, 1983; Dye and Baumgardner, 1984; Cooper, 1988). The presence of ice, at least in very high concentrations, can also lead to error in FSSP measurements (Gardiner and Hallett, 1985). Further difficulties arise when hot-wire devices are used. For example, Spyers-Duran (1968) noted that the collection efficiency of the sensor wire is dependent on drop size and Strapp and Schemenauer (1982) recognized that the buildup of ice on the sensor head can lead to measurement error. Therefore, the quality of data on supercooled cloud droplets has first been assessed.

Table 2. Summary for Supercooled Cloud Droplets at T ≈ -10°C.

C_ID	U_ID	PJWC g m^{-3}	MJWC g m^{-3}	PFWC g m^{-3}	MFWC g m^{-3}	DBAR μm	MCONC cm^{-3}	PCONC cm^{-3}
708c1	1	0.4	0.3	0.4	0.4	14	152	162
	2*	0.7	0.5	0.5	0.4	12	205	258
	3	0.7	0.5	0.5	0.4	14	167	243
708c3	4*	0.1	0.0	0.3	0.2	16	65	169
	5	0.0	0.0	0.1	0.1	23	12	13
	6	0.1	0.1	0.3	0.2	14	93	145
	7	0.0	0.0	0.1	0.1	22	11	13
	8	0.0	0.0	0.0	0.0	14	10	97
708c5	9*	2.3	1.2	0.8	0.5	14	209	253
	10	1.3	1.1	0.6	0.6	15	189	210
	11	0.8	0.5	0.4	0.4	14	140	160
	12	0.2	0.1	0.2	0.2	12	81	120
	13	0.2	0.1	0.3	0.1	18	48	101
708c7	14	0.3	0.2	0.3	0.2	13	102	139
	15	0.2	0.1	0.4	0.3	18	57	87
	16*	0.1	0.0	0.3	0.2	16	46	106
	17	0.1	0.1	0.2	0.1	10	89	146
708c11	18*	0.2	0.1	0.2	0.1	4	24	96
	19	0.3	0.2	0.3	0.2	12	103	157
	20	2.2	1.1	0.6	0.5	14	191	247
	21	1.5	1.2	0.5	0.4	14	176	244
708c12	22	0.0	0.0	0.2	0.2	23	16	16
	23	0.1	0.0	0.2	0.1	18	31	109
	24*	0.1	0.0	0.1	0.1	22	9	39
708c14	25	0.5	0.4	0.5	0.4	13	166	229
	26*	0.3	0.2	0.4	0.3	16	90	114
	27	0.4	0.3	0.5	0.3	15	114	141
724c1	28*	0.5	0.3	0.5	0.4	14	126	172
	29	0.2	0.1	0.3	0.2	14	71	125
	30	0.6	0.3	0.5	0.3	14	135	183
	31	0.8	0.2	0.5	0.2	16	81	166
724c5	32	0.8	0.7	0.6	0.6	15	224	234
	33	0.6	0.6	0.6	0.5	14	219	226
	34*	1.5	0.9	0.8	0.7	15	259	335
	35	0.9	0.7	0.7	0.5	14	239	291
724c7	36*	2.3	1.6	0.7	0.6	14	287	345
	37	1.8	1.5	0.5	0.4	13	234	288
	38	0.3	0.2	0.3	0.2	13	96	169
724c8	39*	0.4	0.3	0.4	0.4	13	188	225
	40*	0.7	0.6	0.6	0.5	14	215	266

* - main updraft

5.2.1 Valuation of the JW and FSSP data

An indication of the performance of the JW and FSSP probes can be obtained by comparing the mean liquid water content (LWC) simultaneously measured by each. Figure 3 is a plot of mean liquid water measured by the JW versus that calculated from the FSSP data. Figure 3 clearly shows that the measurements of mean LWC are in fairly good agreement for values less than 0.5 g m^{-3}; this is also true for the instantaneous 1-second values. However, for values greater than 0.5 g m^{-3} the FSSP does not show increases corresponding to those indicated by the JW.

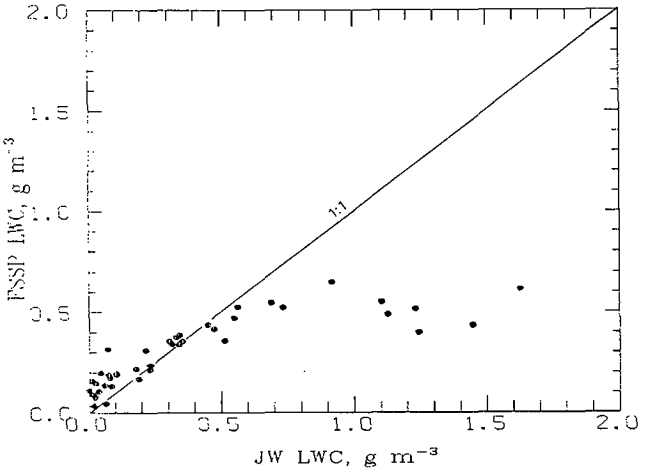

Figure 3. Comparison of JW and FSSP liquid water measurements.

Several explanations for this discrepancy have been explored, but none have strong support in the data. First considered was the possibility that the discrepancy was associated with sampling in regions with large amounts of supercooled drizzle and raindrops. Sampling in such regions could lead to fogging of the FSSP optics and thus result in an artificially low FSSP LWC. Another related possibility is that icing on the probes may result in JW LWCs which are too high, or FSSP LWCs which are too low, or both. Finally, if the size spectrum of large supercooled drops happened to contain high concentrations of drops near 50 μm in diameter, the JW probe may simply have intercepted a few small precipitation-size drops that may not be detected by the FSSP (i.e., the detectable size range of the JW is slightly greater than that of the FSSP). However, when the data were examined for differences between mean JW LWC and FSSP LWC for each updraft as compared to the drop information from the 2D probes, no such tendency was found for the discrepancy to

occur with 2D water parameters such as 1) net 2D liquid water, 2) 2DC liquid water, or 3) the slope or intercept of the drop size spectrum.

Further examination of the data (see Table 2) revealed that the discrepancy coincided with the occurrence of the highest concentration of cloud droplets as indicated by the FSSP. For the six measurements of MJWC in excess of 1.0 g m^{-3} (updrafts 36, 37, 21, 9, 10, and 20) and the remaining eight between 0.5 and 1.0 g m^{-3} (updrafts 34, 35, 32, 33, 40, 2, 3, and 11), FSSP cloud droplet concentrations were among the highest. Since the FSSP seems to be responding to the presence of the largest number of drops, fogging seems unlikely unless just the measurement of drop diameter was affected. However, no difference in mean FSSP drop diameters seems to be associated with the JW FSSP discrepancy (as can be seen in Table 2). This finding still leaves the possibility that the high cloud droplet concentrations were anomalously associated with the presence of ice.

Therefore the difference between JW and FSSP LWC was plotted against total mean concentration of graupel; this plot is shown in Fig. 4. Now in addition to the original discrepancy, a second is revealed which is associated with the amount of ice present, as indicated by the solid line fit to the data. First, in Fig. 4 there are six updrafts (two nearly identical LWC values are plotted near 1.0, 0.0) which had large (> 0.4) positive disagreements that seem to have occurred when mean ice

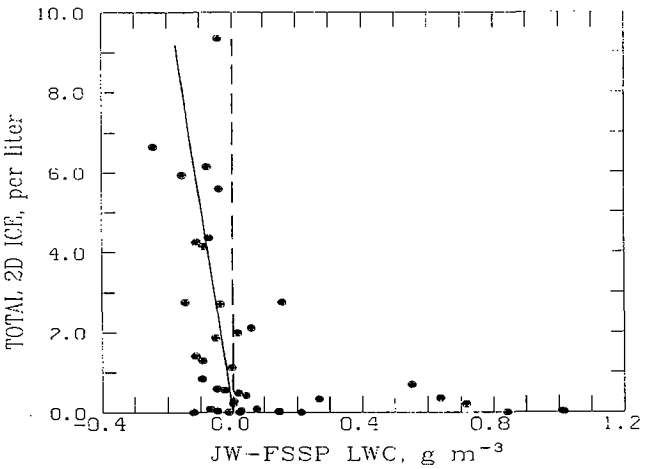

Figure 4. Difference between JW and FSSP liquid water measurement versus total 2D graupel concentration.

concentrations were less than 1 ℓ^{-1}. These are the same six measurements which suggested that the FSSP response flattened above 0.5 g m^{-3}. Secondly, and perhaps more importantly, the data show a slight tendency for FSSP LWC to increasingly exceed JW LWC as mean ice concentration increases. Such discrepancies have been noted before (Gardiner and Hallett, 1985), but not for such low concentrations of ice. Therefore, liquid water contents indicated by the JW have tended to be used when needed in this analysis because FSSP liquid water contents increasingly disagree with the JW at values greater than 0.5 g m^{-3} and because there is some evidence that the FSSP measurements were degraded by the presence of ice.

5.2.2 Character of the supercooled cloud droplet population

The amount of supercooled water in that portion of the size spectrum representing drops smaller than about 50 μm diameter measured less than expected from previous observations of more vigorous midwestern clouds at warmer temperatures (Ackerman *et al.*, 1978). Table 2 shows that most updrafts had at least some supercooled liquid water in the form of cloud droplets. On average the amount of mean liquid water in the updrafts of young clouds calculated from the FSSP was 0.3 g m^{-3} ($\sigma = \pm .2$) and ranged from 0.1 to 0.7. In comparison, mean liquid water content measured using the JW was more broadly distributed than that for the FSSP, ranging from 0 up to 1.2 g m^{-3}; reflecting the tendency for discrepancy between the two probes when liquid water exceeded 0.5 g m^{-3}. However, mean liquid water from the JW averaged 0.4 g m^{-3} which is close to that for the FSSP. Mean concentrations of cloud droplets (MCONC) for young clouds ranged from about 10 to almost 300 cm^{-3} and averaged 135 cm^{-3} (σ = 76). These concentrations are much less than the excesses of 500 cm^{-3} reported for Florida cumulus at the -9°C level (Hallett *et al.*, 1978).

An interesting feature of the supercooled cloud droplet data is the high degree of structure shown in the size spectrum over each cloud transect. Figure 5 shows an example of the variation in droplet concentration and liquid water content constructed from the FSSP data for cloud 708c1p1, along with the cloud's vertical wind profile. The concentration diagram at the top of Fig. 5 clearly shows a bimodal structure with a unimodal distribution at either cloud edge, while the water mass is unimodal and centered at about 21 μm. Thus, even though the size distribution is bimodal, the

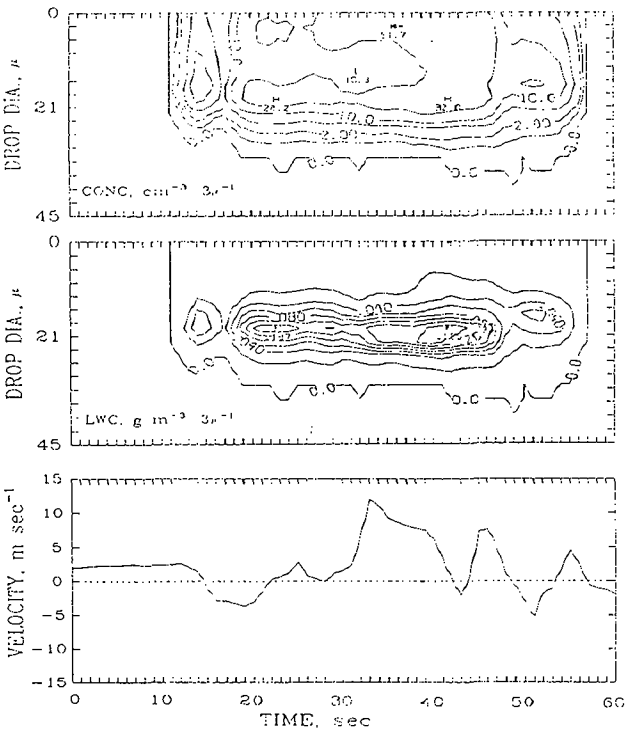

Figure 5. FSSP droplet concentration, liquid water content, and vertical wind calculation for cloud 708c1p1.

expected heat release from intentionally freezing these droplets can be expected to be fairly uniform across the cloud transect.

Warner (1969) has postulated that entrainment may produce a bimodal distribution by evaporating droplets when dry environmental air initially mixes with a cloudy parcel. This event must be followed by condensation growth as the parcel resaturates as a result of droplet evaporation and adiabatic cooling. A bimodal distribution is finally produced when undiluted cloudy air mixes with the entrained parcel and reintroduces the smallest droplets. The unimodal structure at each cloud edge gives an indication that cloud top rather than lateral entrainment is more pronounced for at least this particular cloud.

5.3 Supercooled drizzle and raindrops

The 2D image records were used to assess for the presence of large supercooled drops in each of the 40 updrafts. As discussed early, it was not possible to determine a precise statistical significance for derived amounts of supercooled water content. Therefore, because of this inability, two methods have been employed to estimate an upper and lower bound to the supercooled water content of each updraft.

In the first method, referred to as the discrete method, the lower bound to the 2D water content was obtained from a single drop size distribution for each updraft having size intervals 200 μm wide. The water mass represented in each size interval was accumulated over all drop sizes up to the largest drop recorded from the image record. Hence water contents is represented by the simple equation:

$$LWC_d = (\pi/6)\times 10^6 \rho_w \times \Sigma D_i^3 N(D_i)\Delta D \qquad (1)$$

where $N(D_i)\Delta D$ is the drop concentration in liters per 200 μm interval, D_i is the drop diameter for the center of each size interval, the parameter i ranges from the first size interval to the largest size having a non-zero concentration, and ρ_w is the density of water. Thus, in this method size intervals with no particle concentration make no contribution to the water content.

Figure 6 shows a typical drop size distribution created from the image record classifications for updraft 1. The dotted line through the data is a non-linear least squares fit. In Method I liquid water is computed directly from the concentrations given for each size interval. As is typified in Fig. 6, it was not uncommon for some of the size categories to be empty, thus making no contribution to the water content. Therefore, method I provides an estimate biased toward the least amount of water content since the lack of drop counts in certain size categories is very likely to be the result of sampling small air volumes rather than indicating a true absence of drops.

In the second method, referred to here as the continuous method, an effort was made to account for the empty size categories by using a least squares fit to the size distribution. The first step was to linearize the data by taking the natural logarithm of each drop concentration. The size versus

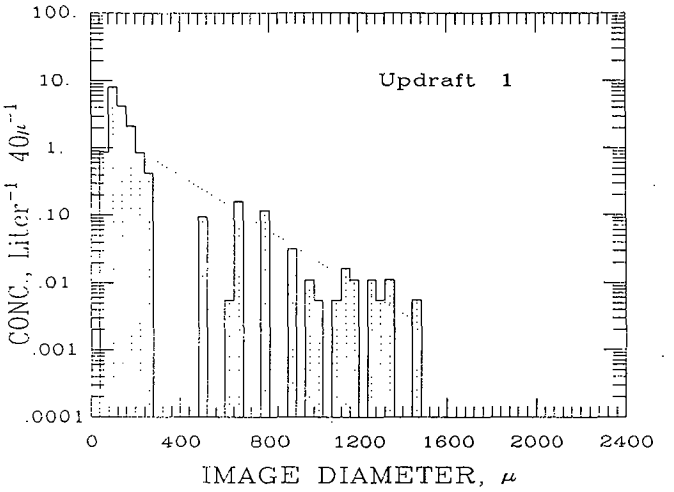

Figure 6. Representative size distribution for 2DC & 2DP images classified as drops for updraft 1.

linearized concentration data were then used in a least squares analysis to obtain an intercept, $\log(N_c)$, and a slope, λ, for the distribution of each updraft. Once these constants are known, the equation:

$$N(D) = N_c e^{-\lambda D} \qquad (2)$$

is satisfied and can be used to approximate the continuous decrease of drop concentration with size.

Recalling that the integral form for liquid water content is:

$$LWC_c = (\pi/6)\times 10^6 \rho_w \int D^3 N(D) dD \qquad (3)$$

substitution of Eq. 2 into Eq. 3 followed by integration of Eq. 3 yields a third order polynomial for water content:

$$LWC_c = -(\pi/6)\times 10^6 \rho_w N_c \lambda^{-1} e^{-\lambda D_C} \times \{D^3+3D^2\lambda^{-1}+6D\lambda^{-2}+6\lambda^{-3}\}\Big|_{D_1}^{D_2} \qquad (4)$$

Since all drop sizes from D_1 to D_2 contribute to the water content, empty categories are accounted for by assuming that the absence of drops in certain size categories occurred by virtue of poor sampling. This is probably not a poor assumption for smaller drops, since coalescence has had a long time to operate and the size distribution should be fairly continuous. However, the largest drops are likely produced probabilistically from "self-collection" (Berry and Reinhardt, 1974). Thus an empty category may just as likely represent an absence of drops as be the result of poor sampling. Since the largest drops make the biggest contribution to the water content, the continuous method should give an idea of the vicinity of the upper bound because the concentration of the largest drops is overestimated to some extent.

Table 3 lists the liquid water content using Eq. 1 (LWC_d) and the liquid water content using Eq.

Table 3. Summary for Supercooled Drizzle and Raindrops at T ≈ -10°C.

U_ID	λ cm^{-1}	N_0 ℓ^{-1}	r	D_{max} μm	LWC_d $g\ m^{-3}$	LWC_c $g\ m^{-3}$	
1	47.2	2.35	-0.90	1460	0.17	1.02	
2	22.0	0.11	-0.80	2660	0.30	1.08	
3	23.6	0.22	-0.83	2460	0.29	1.58	
4*	23.8	0.18	-0.83	2620	0.30	1.32	
5*	32.4	1.36	-0.75	1900	0.29	2.76	
6*	30.7	0.54	-0.85	2260	0.28	1.47	
7*	27.5	0.58	-0.85	1820	0.25	1.97	
8*	--	--	--	--	--	--	PF
9	21.6	0.04	-0.73	2900	0.04	0.47	
10	27.5	0.40	-0.83	1620	0.12	1.20	
11	30.4	0.70	-0.83	1460	0.12	1.39	
12	15.9	0.09	-0.81	2380	0.22	2.17	
13	13.4	0.04	-0.73	1940	0.14	0.93	
14	36.1	0.24	-0.80	1020	0.02	0.18	
15	23.6	0.24	-0.71	1140	0.15	0.59	
16	56.2	2.26	-0.92	1140	0.06	0.45	
17	54.9	3.82	-0.84	1140	0.07	0.83	
18	--	--	--	--	--	--	PF
19	68.6	0.84	-0.94	900	0.01	0.07	
20	22.6	0.36	-0.76	2820	0.23	3.35	
21	--	--	--	--	--	--	PF
22	5.4	0.13	-0.45	1460	0.37	4.07	
23	3.8	0.02	-0.27	1980	0.24	2.71	
24	--	--	--	--	--	--	PF
25	33.5	0.18	-0.82	1140	0.04	0.20	
26	2.9	0.06	-0.16	1020	0.09	0.62	
27	17.5	0.05	-0.71	1140	0.03	0.21	
28*	6.3	0.03	-0.60	3460	1.01	9.74	
29*	7.5	0.13	-0.76	2820	2.23	20.31	
30*	3.2	0.02	-0.27	2700	1.34	7.98	
31*	5.0	0.03	-0.30	2420	0.44	4.29	
32	2.5	0.04	-0.27	1620	0.17	2.84	
33	--	--	--	1580	0.21	--	IN
34	86.3	2.10	-0.97	700	0.01	0.06	
35	--	--	--	--	--	--	PF
36*	--	--	--	1620	0.03	--	PF
37*	4.6	0.02	-0.58	2020	0.12	1.76	
38*	--	--	--	1660	0.11	--	IN
39	--	--	--	700	0.02	--	IN
40	64.2	5.16	-1.00	780	0.03	0.48	

* - main updraft
PF - Probe failure
IN - Insufficient number of images

4 (LWC_c) computed over the size range from D=50 μm (to approximately match where the FSSP leaves off) up to D_{max} for each updraft. Table 3 also lists the slope (λ, cm^{-1}), drop concentration at the intercept (N_0, per liter per 40 μm interval at D=0), and the correlation coefficient for each least squares fit, along with the largest (D_{max}) drop size recorded.

The dotted line in Fig. 6 shows the fit to the distribution determined in the continuous method. Smaller correlation coefficients listed in Table 3, correspond to large scatter and fewer images. It was not possible to compute LWC_c for several updrafts for reasons related to probe hardware failure (PF) or because an insufficient number (IN) of size categories were filled for the least squares fit (in this analysis at least 4 were required).

The largest water content, which was computed for cloud 724c1p1 updraft 29, is in excesses of the adiabatic amount. Clearly, a liquid water content of this magnitude is suspect. However, we are at a loss to explain this unusually large value. Nevertheless, we have excluded the cloud 724c1p1 in subsequent parts of the analysis that require liquid water content from large drops.

The mean liquid water content for supercooled drizzle and raindrops in the updrafts of "young" clouds was 0.13 g m^{-3} with a standard deviation of 2.21, computed from values determined in the discrete method. Corresponding values computed from the continuous method are 1.20 g m^{-3} and 23.37, respectively. Maximum and minimum amounts are 0.37 and 0.01 for the discrete method, and 4.07 and 0.06 for the continuous method.

Figure 7 shows a cumulative frequency distribution for the fraction of precipitation water content relative to the total water content. The distribution was created from liquid water data from the FSSP by using the discrete method applied to the 2D data for each updraft of the young clouds. It can be inferred from Fig. 7, as was done in previous studies (Ackerman *et al.*, 1978), that a substantial amount of water in the updraft is in the size range of drizzle and raindrops. For example, 20% of the updrafts had 50% or more of their water mass content composed of drizzle and raindrops, and 50% of the updrafts had approximately 25% or more of their mass content composed of drizzle and raindrops. Thus, for warm-based clouds with moderate updrafts, liquid water content as indicated by the FSSP or hot-wire probe is insufficient for characterizing the supercooled water content in establishing cloud suitability for seeding.

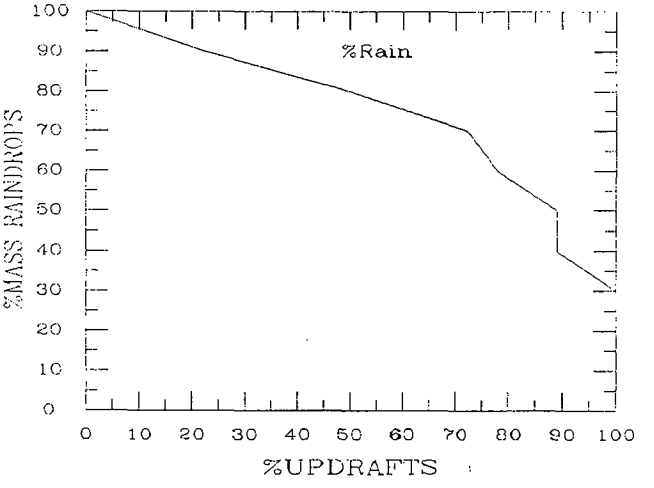

Figure 7. Cumulative frequency distribution for the percent mass of liquid water in the form of drizzle and raindrops.

Even though we do not have precise values for liquid water content, these data provide good evidence that a "warm" coalescence process must occur above the melting level along with glaciation. This fact for warm-based clouds has often escaped attention in considerations of precipitation production and probably should not continue to be overlooked. Time for coalescence to operate allows drops to coincidentally increase in size with ice as cloud evolves, assuming, of course, that coalescence efficiency is not negatively influenced by a change in deformation that may accompany changes in surface tension and fall speeds with temperature and pressure. Hence, a rapid creation of liquid and solid particles can be expected that is large enough to fall against the updraft and thus return the water toward earth, even though the cloud may be growing vigorously.

The implication for dynamic cloud seeding may be important because the possibility exists to halt the collection process, "freezing" the size spectrum while simultaneously invigorating the updraft from latent heat release. The manifestation of such an occurrence may be suggested in the documentation of cloud-top "cut-off" following seeding (see, for example, Simpson and Dennis, 1974). Furthermore, net reductions in rainfall (at least for large clouds) have also been suggested in numerical evaluations of seeding effects on warm-based clouds (Orville et al., 1989). In these evaluations, it is suspected that the cause of the rain decrease is the glaciogenic origination of ice crystals that are transported aloft and carried away. Thus, for a cloud to be suitable for dynamic seeding, it must contain supercooled drizzle and raindrops not only for the latent heat they contain, but also for the brake they apply to the updraft so that water is not directed to upper tropospheric levels and transported away.

5.4 Ice

The 2D image records were also used to make an assessment of the kind and amount of ice in the updraft of this sample. Ice particle images were classified as either graupel, vapor-grown ice crystals, aggregates, or crystal fragments. An image was classified as graupel if it had a fairly complete, quasi-spherical or conical shape with ragged outline. An image must have shadowed at least 6 diodes along either the major or minor axis for the raggedness of the outline to be discernible. Images were classified as ice crystals when their shape resembled that of either a complete needle, column, stellar, dendritic, or hexagonal form. An image was classified as a fragment if it had the appearance of part of one of the above ice crystal types, most typically the shape of one or more arms from a stellar form.

Table 4 summarizes estimates about the ice content of each updraft for each probe. Listed by updraft identification number (U_ID) for the 2DC and 2DP probes are the concentration of graupel (N_g) per 40 μ size interval, and solid water content (SWC_d). Total concentration (TN_g) and solid water content ($TSWC_d$) are also given in Table 4. Summary of estimates for images that may have been created by pristine ice crystals, fragments or aggregates are not given since concentrations of these are generally zero or less than 0.01 ℓ^{-1} for particles greater than 150 μm diameter. Table 4 also provides for each updraft concentrations of supercooled cloud droplets with diameters less than 15 μm ($N_{<15}$) and greater than 24 μm ($N_{>24}$) along with g(r) which is the ratio of the concentration of cloud droplets less than 15 μm to the total cloud droplet concentration.

To make an estimate of the solid water content, it was necessary to make an assumption about the shape of the graupel size distribution. Therefore, as was done for images that resembled supercooled drops, size distributions were constructed and inspected for each updraft. As shown in Fig. 8, some ice distributions are rather well developed and thus assuming an exponential decrease in concentration with size may be an acceptable way to estimate solid water content. However, in the more usual case, shown in Fig. 9, the distribution is not as well developed as in Fig. 8. Thus, because so many of the size distributions

Table 4. Summary of Estimates for Ice at T ≈ -10°C.

				2DC		2DP		2DC+2DP	
U_ID	$N_{<15}$ cm^{-3}	$N_{>24}$ cm^{-3}	g(r)	N_g ℓ^{-1}	SWC_d g m^{-3}	N_g ℓ^{-1}	SWC_d g m^{-3}	TN_g ℓ^{-1}	$TSWC_d$ g m^{-3}
1	90	4	0.21	11.1	0.21	0.08	0.03	11.18	0.24
2	137	5	0.21	3.9	0.10	0.11	0.20	4.01	0.30
3	108	6	0.24	4.1	0.08	0.09	0.23	4.19	0.31
4*	50	4	0.25	8.1	0.16	0.12	0.34	8.22	0.50
5*	3	4	0.06	8.5	0.14	0.07	0.09	8.57	0.23
6*	73	4	0.36	3.4	0.05	0.09	0.21	3.49	0.26
7*	3	3	0.07	8.6	0.18	0.11	0.32	8.92	0.50
8*	7	1	0.17	----	----	----	----	----	----
9	117	4	0.23	1.4	0.01	0.01	0.01	1.41	0.02
10	90	5	0.18	1.6	0.02	0.08	0.06	1.68	0.08
11	90	5	0.25	6.4	0.06	0.08	0.02	6.48	0.08
12	65	4	0.30	7.5	0.00	0.12	0.16	7.62	0.16
13	32	3	0.25	0.0	0.00	0.06	0.21	0.06	0.21
14	69	2	0.32	2.3	0.01	0.17	0.00	2.47	0.01
15	30	11	0.13	26.6	0.04	0.08	0.01	26.68	0.05
16	30	6	0.17	27.6	0.07	0.10	0.02	27.70	0.09
17	78	4	0.32	18.4	0.08	0.09	0.04	18.49	0.12
18	15	0	0.24	----	----	----	----	----	----
19	75	2	0.24	0.0	0.00	----	----	0.00	0.00
20	111	5	0.23	4.7	0.00	0.19	0.36	4.89	0.36
21	106	4	0.26	----	----	----	----	----	----
22	3	5	0.05	0.0	0.00	0.00	0.00	0.00	0.00
23	22	3	0.14	0.0	0.00	0.15	0.33	0.15	0.33
24	3	3	0.05	----	----	----	----	----	----
25	120	6	0.34	1.9	0.01	0.00	0.00	1.90	0.01
26	50	7	0.21	3.1	0.02	0.00	0.00	3.10	0.02
27	66	7	0.22	2.2	0.01	0.00	0.00	2.20	0.01
28*	73	5	0.19	2.5	0.07	0.21	1.16	2.71	1.23
29*	50	4	0.32	24.7	0.09	0.63	1.45	25.33	1.54
30*	88	5	0.30	3.2	0.01	0.22	1.21	3.42	1.22
31*	47	6	0.21	4.5	0.00	0.17	0.41	4.67	0.41
32	124	3	0.26	0.0	0.00	0.04	0.03	0.04	0.03
33	122	3	0.25	3.7	0.01	0.03	0.05	3.73	0.06
34	139	4	0.24	1.3	0.01	0.01	0.01	1.31	0.02
35	140	2	0.30	----	----	----	----	----	----
36*	177	3	0.32	----	----	0.03	0.01	0.03	0.01
37*	161	1	0.42	0.0	0.01	0.12	0.06	0.12	0.07
38*	67	0	0.43	0.0	0.01	0.04	0.12	0.04	0.13
39	123	1	0.30	15.5	0.12	0.10	0.07	15.60	0.18
40	117	2	0.29	0.0	0.00	0.16	0.31	0.16	0.31

* - main updraft

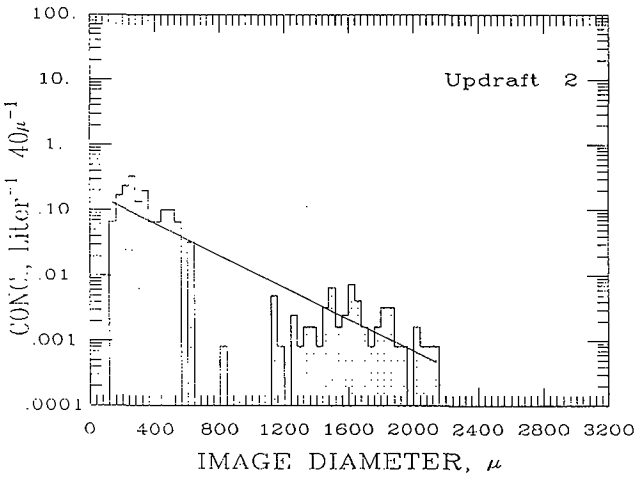

Figure 8. Representative size distribution for images classified as graupel for updraft 2.

are not very well filled, estimation of the solid water content in Table 4 has been limited to use of the discrete method described by Eq. 1, using ρ_i of 0.9 g cm^{-3} for high-density ice.

As was the case when this method was used to infer liquid water content from the 2D data, underestimation of true ice amounts is likely. Further underestimation may have occurred because vapor-grown ice crystals were not included in the estimate. However, underestimates in mass related to the exclusion of ice crystals may not be that great because few ice crystals were identified in the 2D records. Instrumentation capable of

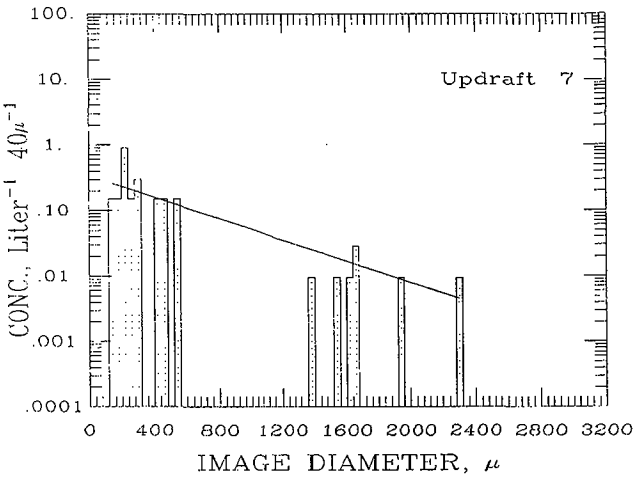

Figure 9. Same as Figure 8, but for updraft 7.

detecting small ice crystals was not available in 1986. If the absence of large vapor-grown ice crystals in this sample of Midwestern updrafts marks the results of natural processes rather than an instrument inadequacy, then an important departure from the conditions in Florida cumulus should be noted. Hallett *et al.* (1978) collected data in clouds at the -4 and -9°C level during the 1975 Florida Area Cumulus Experiment (FACE) and reported several cumulus that produced vapor-grown ice in concentrations in excess of 10 ℓ^{-1}. Therefore, future determination of the initial general presence or absence of vapor-grown crystals may point to an important difference in the precipitation processes of Midwestern and Florida cumuli and to possible differences in expected alteration and perhaps reaction to seeding.

As can be seen in Table 4 and in keeping with results from Project Whitetop (Braham, 1964) and FACE (Hallett *et al.*, 1978), virtually all of the updrafts contained some amount of graupel, often in concentrations larger than would be expected if the ice originated solely from ice nuclei present in conventional concentrations. Eighteen of the 23 young-cloud updrafts for which complete 2DC and 2DP records are available had total concentrations greater than 1 ℓ^{-1}, when approximately 0.01 ℓ^{-1} would be conventionally expected from ice nuclei (Fletcher, 1962). In five instances total graupel concentrations in young-cloud updrafts were computed to be in excess of 10 ℓ^{-1}. Five young-cloud updrafts total graupel concentrations less than 1 ℓ^{-1} and there was one updraft that apparently had no ice at all. Further inspection of Table 4 shows that 2DC graupel concentration dominate. However, the mass contribution to the condensate load is about the same from each probe.

Because graupel was observed in concentrations greater than conventionally expected from ice nuclei, the question arises as to whether or not a secondary or ice multiplication process, such as rime-splintering, operated in these updrafts (Hallett and Mossop, 1974). A Hallett-Mossop process is first suspected since qualitatively the criteria necessary for this mechanism have been met. For example, the air of these updrafts rose through the -3 to -8°C layer (Hallett and Mossop, 1974), and as indicated in Table 4, concentrations of small (D < 13 μm) and large (D > 24 μm) droplets also typically existed (Mossop and Hallett, 1974; Mossop, 1976; Mossop, 1978).

To more objectively address this question, a simple model was developed to compute ice concentrations expected at -10°C if a rime-splintering process operated. If expected ice concentrations are in good agreement with concentrations observed at -10°C, then evidence exists that does not contradict the hypothesis that a rime-splintering process operated. The model that has been developed to compute expected ice concentrations is based on the simple equation:

$$N_{eI} = \tau \int f(T)m(T)dT \qquad (5)$$

where τ is the time it takes to pass through the -3 to -8°C ice multiplication zone, obtained from $\Delta Z/U$ where ΔZ is the thickness of the -3 to -8°C layer and U is the mean observed updraft velocity which is assumed to be uniform through the layer. The unitless triangular shaped function f(T) represents the temperature dependence of splinter production that has been determined in the laboratory (Mossop, 1976); it is zero at -3 and -8, and unity at -5°C.

In Eq. 5, the function m(T) takes into account changes in microphysical conditions that might influence net splinter production and has units particles per cubic meter per second. This function accounts for increases in production rate that should occur as the graupel population grows in size and concentration with parcel ascent to colder temperatures, and accounts for decreases in production rate that should occur from depletion of cloud droplets (both smaller than 13 and greater than 25 μm diameter) by riming, perhaps entrainment, and other factors.

The approach for calculating expected ice concentration requires that an assumption be made about the form of m(T). Three separate calculations have been performed, one assuming that m(T) takes on a linear form, another assuming m(T) is exponential and lastly another in which m(T) is assumed to have a parabolic form. To illustrate the model, the following discussion assumes that m(T) varies parabolically as:

$$m(T) = C_1T^2 + C_2 \qquad (6)$$

where C_1 and C_2 are constants and T is temperature.

To obtain all the information needed to integrate Eq. 5 values for C_1 and C_2 need to be determined. The constants C_1 and C_2 can be found if the following assumptions are made: 1) m(T) is zero at -3°C; and 2) m(T) = IIPR at -10°C, where IIPR is the instantaneous ice production rate defined by the equation:

$$IIPR = Cf(T)\iint g(r)\pi(R_g+r)^2\times$$

$$[V(R_g)-v(r)]N(R_g)n(r)E(R_g,r)dR_gdr \qquad (7)$$

In Eq. 7 (originally derived by Harris-Hobbs and Cooper, 1987) R_g, $N_g(R_g)$, and $V(R_g)$ are radius, size spectrum, and fall speed for graupel, respectively. The variables r, n(r), and v(r) are respectively, cloud droplet radius, size spectrum, and fall speed. In Eq. 7 the function g(r) represents the ratio of

the concentration of supercooled droplets less than 15 μm to the total concentration of cloud droplets as indicated by the FSSP. The collection efficiency E(Rg,r) is that for collisions between graupel and cloud droplets, and was taken as unity in these calculations. The constant C was given as 0.16 in Harris-Hobbs and Cooper (1987) and was determined by fitting Eq. 7 to the laboratory data of Mossop (1978). Values for the fall speed for graupel and drops can be obtained from relationships provided by Heymsfield (1978) and Beard (1976), respectively. Therefore, C_1 and C_2 can be found from a simple system of two equations and two unknowns.

There currently exists no strong scientific basis to prefer a linear, parabolic, or exponential form for m(T). However, some inclination can be given toward a parabolic form because a Hallett-Mossop process might be expected to start out slowly, continue that way for a while, and then accelerate rapidly as is implicit in some of the modeling output of Scott and Hobbs (1977).

Table 5 lists expected ice concentrations computed by integrating Eq. 5 from -5 to -8°C and assuming the m(T) is linear (N_L), parabolic (N_P) and exponential (N_E). Expected concentrations were only computed if data from both the 2DC and 2DP probes were available. Table 5 also lists for each updraft the observed ice concentration (N_I), the instantaneous ice production rate (IIPR) computed by using Eq. 7, the mean updraft velocity (U) and the mean time for transit through the -3 to -8°C rime-splintering zone (τ). Means (μ) and standard deviations (σ) for each column are listed along the bottom of Table 5 for all, young, and older-cloud updrafts.

As can be seen in Table 5 on average expected ice concentrations are in excess of observed for both young and older-cloud updrafts. Expected ice concentrations assuming that m(T) has a parabolic form are in closer agreement than those assuming either a linear or exponential form. The apparent agreement between the expected ice concentrations assuming linear and exponential forms for m(T) has probably resulted because integration over a short interval on an exponential curve is approximately linear.

Considering the simplicity of the expected ice concentration model and the large measurement uncertainty associated with 2D and FSSP measurements, agreement between observed and expected ice concentrations (N_P) is surprisingly good if, in fact, m(T) varies parabolically. Of the 33 updrafts for which the computation was made the descrepancy was positive ($N_P > N_I$) for 23 and negative for 10. This tendency for expected to exceed observed concentrations is consistent with the possibilty that small ice (D < 150 μm) was present but went undetected. Thus, the hypothesis that a rime-splintering process may have operated in these updrafts is not contradicted, assuming m(T) varies parabollically. However, because support for this assumption is not firm, alternate hypothesis such as the possibility that either a rime-splintering process did not operate, in favor of other mechanism(s), or that rime-splintering operated less efficiently than expected from the microphysical conditions can not be precluded. Future observational study of ice initiation in summer convective clouds must (1) obtain data on small ice content, (2) measure ice nuclei concentrations, and (3) circumvent the problem of aircraft produced air

Table 5. Observed and Expected Ice Concentrations.

	U_ID	Observed N_I ℓ^{-1}	IIPR $m^{-3}\ s^{-1}$	U $m\ s^{-1}$	τ s	Expected N_L ℓ^{-1}	N_P ℓ^{-1}	N_E ℓ^{-1}
	1	11.18	108.00	1.05	915.7	87.13	32.93	86.18
	2	4.01	128.00	6.14	156.6	17.66	6.67	17.32
	3	4.19	154.00	4.28	224.6	30.48	11.52	29.59
	4 *	8.22	227.00	3.52	273.2	54.63	20.65	51.85
	5 *	8.57	36.00	.85	1131.2	35.88	13.56	36.83
	6 *	3.49	139.00	1.53	628.4	76.96	29.09	75.13
	7 *	8.92	33.00	.73	1317.1	38.29	14.47	39.35
	8 *	-----	-----	2.37	405.7	-----	-----	-----
	9	1.41	18.00	6.69	143.7	2.28	.86	2.32
	10	1.68	87.00	5.09	188.9	14.48	5.47	14.47
	11	6.48	125.00	5.07	189.6	20.88	7.89	20.50
	12	7.62	243.00	3.34	287.9	61.63	23.29	58.26
	13	.06	52.00	2.97	323.7	14.83	5.61	15.11
	14	2.47	30.00	5.60	171.7	4.54	1.72	4.66
	15	26.68	86.00	7.81	123.1	9.33	3.53	9.33
	16	27.70	129.00	5.88	163.5	18.58	7.02	18.22
	17	18.49	132.00	2.68	358.8	41.72	15.77	40.84
	18	-----	-----	1.61	597.2	-----	-----	-----
	19	-----	-----	2.07	464.5	-----	-----	-----
	20	4.89	478.00	7.04	136.6	57.51	21.74	52.13
	21	-----	-----	2.09	460.0	-----	-----	-----
	22	-----	-----	1.10	874.1	-----	-----	-----
	23	.15	81.00	1.55	620.3	44.27	16.73	44.38
	24	-----	-----	3.54	271.6	-----	-----	-----
	25	1.90	11.00	11.27	85.3	.83	.31	.82
	26	3.10	27.00	10.07	95.5	2.27	.86	2.33
	27	2.20	9.00	8.48	113.4	.90	.34	.87
	28 *	2.71	602.00	12.11	79.4	42.11	15.92	37.62
	29 *	25.33	161.00	6.19	155.3	22.03	8.33	21.33
	30 *	3.42	573.00	7.30	131.7	66.49	25.13	59.58
	31 *	4.67	243.00	7.47	128.7	27.56	10.42	26.05
	32	.04	20.00	1.58	608.5	10.72	4.05	10.97
	33	3.73	42.00	1.94	495.6	18.34	6.93	18.78
	34	1.31	11.00	1.53	628.4	6.09	2.30	6.01
	35	-----	-----	2.31	416.2	-----	-----	-----
	36 *	.03	56.00	5.74	167.5	8.26	3.12	8.40
	37 *	.12	42.00	4.85	198.2	7.34	2.77	7.51
	38 *	.04	5.00	2.38	404.0	1.78	.67	1.53
	39	15.60	44.00	2.28	421.7	16.35	6.18	16.73
	40	.16	91.00	2.75	349.6	28.03	10.60	27.95
all	μ	6.38	127.97	4.78	346.0	26.97	10.20	26.15
	σ	7.83	152.20	3.06	304.4	23.53	8.90	22.45
young	μ	6.59	95.73	4.78	309.2	23.13	8.74	22.63
	σ	8.27	103.80	2.92	221.9	22.62	8.55	21.79
older	μ	5.96	192.45	4.79	419.5	34.67	13.10	33.29
	σ	7.25	211.29	3.46	429.3	24.51	9.26	23.13

* - main updraft

particles (Rangno and Hobbs, 1983; Rangno and Hobbs, 1984), as additional steps needed for determining the mechanism(s) of ice generation.

Although the matter of whether or not a Hallett-Mossop process operated in this sample of Midwestern clouds remains unsettled, it is still of interest to note that the effect of entrainment (suggested in Fig. 5) to change the shape of the cloud droplet size distribution may not necessarily work against a rime-splintering mechanism. Recall that laboratory experiments indicate that it is necessary for a cloud to contain droplets greater than or equal to 25 μm (Mossop and Hallett, 1974) as well as droplets smaller than or equal to 13 μm for a rime-splintering process to be effective. In Fig. 5, it can be seen that these size ranges are almost absent at cloud edge and pronounced within cloud where entrainment is inferred. Thus, since droplets smaller than 13 μm and larger than 25 μm are still present (and perhaps in enhanced concentrations) after entrainment, secondary ice production by rime-splintering is not necessarily adversely affected. Hence, although entrainment is generally thought to have a negative impact on overall cloud development, it may not necessarily be detrimental to the Hallett-Mossop process.

An additional, exploratory test relevant to the possible operation of a rime-splintering process has been made on the basis of graupel size and updraft criteria implicit from the work of Mossop (1976). From this work it was reported that the

rate of splinter production is not sensitive to the velocity of the riming body over the velocity range from 1.4 to 3 m s^{-1}. This suggests that an optimum relationship exists between updraft velocity and graupel fall speed (size) to optimize the amount of time spent in transit through the ice multiplication zone and thus result in peak ice splinter production.

For the case of initial secondary ice production, transit time in the rime-splintering zone need only be considered. Thus, initial ice production is represented by the observations presented herein which were collected shortly after cloud top passed through flight level, and hence particle sedimentation from colder temperatures aloft was mostly absent. Under these circumstances, if the velocity of the updraft is too fast and the fall speed of the rimers is too slow, then the riming particles will be carried rapidly through the multiplication zone without much splinter production. Conversely, it may be hypothesized that if the updraft velocity is too slow and the rimers too large (i.e., falling fast) then the graupel will fall out of the zone, resulting in little splinter production. Therefore, it might be suspected that when the fall speed of the graupel is close to that of the updraft velocity, "fountaining" of the rimers occurs and much time is spent in the splinter production zone.

To test this hypothesis, a non-dimensional number was developed to gain a sense for the fall velocity of the rimers relative to the updraft. A characteristic graupel mass (M*) was determined from the ratio of total solid water content ($TSWC_d$) to total ice concentration ($TCONC_d$) written as:

$$M^* = TSWC_d/(TCONC_d \times 1000) \qquad (7)$$

where $TSWC_d$ has units g m^{-3}, and the total ice concentration ($TCONC_d$) has units ℓ^{-1}. From the mass a characteristic diameter (D*) was obtained assuming high-density ice (ρ_i = 0.90 g cm^{-3}). Once D* is known, the characteristic fall speed (V_T*) of the rimers can be estimated by using the relationship given by Heymsfield (1978) extrapolated down into the sub-millimeter size range.

The fountain point (η_{FP}) is written as:

$$\eta_{FP} = (U_m - V_T^*)/U_m \qquad (8)$$

where U_m is the mean updraft velocity and V_T is the characteristic fall speed of the graupel calculated from D*. Thus, Eq. 8 represents the vertical progress of the ice. When it is zero, the updraft velocity balances the fall speed of the graupel and a "fountaining" of the particles in the updraft can be envisioned: the particles progress neither upward nor downward. As η_{FP} approaches unity, particle transport upward at nearly the speed of the updraft is indicated. η_{FP} can never be greater than unity, and negative values indicate sedimentation.

Fountain points have been computed and are plotted in Fig. 10 as a function of graupel concentration. Solid squares indicate updrafts in young clouds, and open triangles indicate updrafts in older clouds. In Fig. 10, we expect to see a

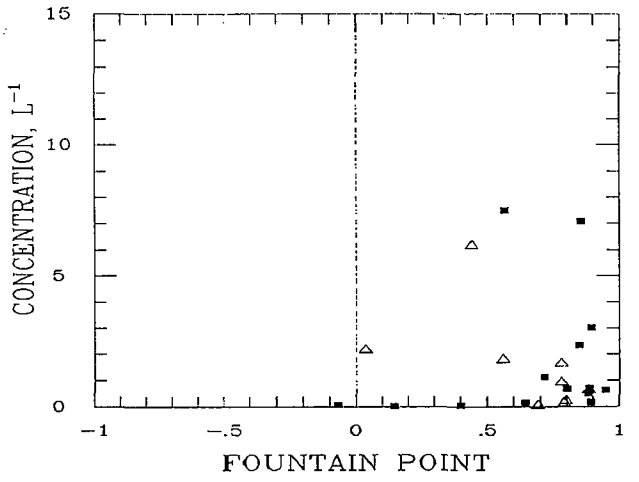

Figure 10. Fountain points versus total graupel concentration.

tendency for higher graupel concentrations to be correlated with fountain points near zero if residence time in the ice multiplication zone is important to rime-splintering. However, in Fig. 10 we see that many of the points lie near $\eta_{FP} \approx 1$, indicating that characteristically for these updrafts the ice is transported in the vertical at a speed nearly equal to that of the updraft. One interpretation is that the process operates efficiently enough not to be sensitive to production time and that updraft-to-updraft variation in ice may be attributed to variation in the favorableness for rime-splintering in the droplet and raindrop spectra.

Although ice was found in concentrations greater than typical ice nuclei concentration, the total mass of water in the liquid state was found to exceed that in the frozen state in all updrafts for which a comparison could be made. Data from the FSSP, 2DC, and 2DP were combined to determine the total liquid water content (TLWC) and solid water content (TSWC) of each updraft. As shown in Fig. 11, all the updrafts had supercooled water contents which were at least as great if not greater than the solid water content. Furthermore, as would be suspected for observations which reflect the production of the very first ice, in the cases where

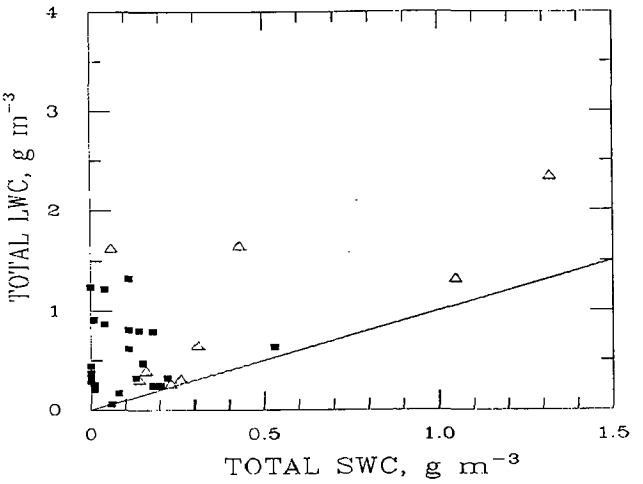

Figure 11. Comparison of total liquid and solid water content for each updraft.

ice solid water contents are very small, liquid water contents are typically large; and when ice contents happen to be large, they are easily matched by the supercooled liquid water content. Thus, even though the ice processes are presumably proceeding more rapidly than a process involving only simple heterogeneous freezing by ice nuclei, the supercooled liquid water content in the initial stage of glaciation is not so overwhelmed as to discount the possibility of alteration of cloud dynamics by glaciogenic seeding.

5.5 Buoyancy and net condensate loading

In addition to the intrinsic value of characterizing properties of the cloud condensate for the purposes of furthering precipitation modeling, knowledge of the condensate load is also required to estimate updraft buoyancy. As is well known, net thermal buoyancy, determined by the moist density difference between the updraft and environment and by the amount of condensate load, can be expressed as:

$$\beta_T = [\theta_v - \theta_v'] - L_{H2O} - L_{ICE} \qquad (9)$$

where the virtual potential temperature of cloud (θ_v) and environment (θ_v') are used to account for parcel moistness and adiabatic temperature variations induced by vertical air motions. Environment temperatures were taken as those at least 1 km away from cloud edge. In the Midwest, a condensate load of 2.5 g m^{-3} is roughly equivalent to -1°C of negative buoyancy for saturated conditions at -10°C. Net loading by the liquid (L_{H2O}) was based on the hot-wire measurements (MJWC) and LWC_d estimates of water contents. Net loading by the ice (L_{ICE}) was based on values given for $TSWC_d$ in Table 4.

Figure 12 shows that the effect of condensate loading on updraft buoyancy can be substantial. In Fig. 12, load-free buoyancies (i.e, $\theta_v - \theta_v'$ only) are plotted as open circles and squares for updrafts in young and older clouds, respectively. The solid symbol connected to the open symbol is the calculated buoyancy, including the weight of the condensate. In Fig. 12, it must be kept in mind

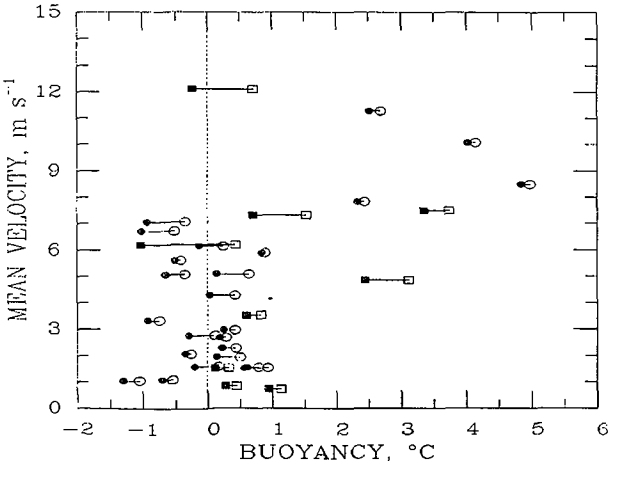

Figure 12. Thermal and net natural buoyancy versus mean updraft velocity.

that estimates of loading are probably underestimated because of the way liquid and solid water contents were estimated.

Although the number of updrafts from older clouds is small, a tendency is evident for loading to be greater in them. On average, water and ice loadings in updrafts of young clouds were -0.22 and -0.04°C, respectively. Similarly, for older clouds loadings are -0.39 and -0.18°C. Loading ratios for ice to water are 0.17 and 0.45 for young and older clouds, respectively. Hence, for this small sample, ice loading becomes about 2.5 times greater as the clouds had time to mature and grow by 5000 ft. Thus, cloud responses to seeding should be fairly sensitive to the stage of cloud development.

5.6 Potential buoyancy enhancement

The effects of glaciation on buoyancy have been a matter of some interest (Saunders, 1957; MacCready and Skutt, 1967; Fukuta, 1973; Orville and Hubbard, 1973); and two mechanisms have been recognized as making a dominant contribution to a temperature change in a glaciating parcel of cloudy air. There is a warming due to latent heat release in the phase change from water to ice, and a warming or a cooling depending on whether deposition or sublimation dominates. The equation found in Orville and Hubbard (1973) for instantaneous isobaric freezing is:

$$\Delta T = T' - T = L_F/c_p W_\ell + L_S/c_p[q_w(T) - q_i(T')] \qquad (10)$$

where T is the parcel temperature before glaciation, T', is the temperature after glaciation, L_F and L_S are the latent heat of fusion and sublimation, W_ℓ is the liquid water expressed as kg water per kg of air, q_w and q_i are the saturation mixing ratio with respect to water and ice, and c_p is the specific heat at constant pressure.

The first term on the right-hand side of Eq. 10 expresses warming from latent heat release in freezing (ΔT_f), and the second term expresses a temperature change related to depositional processes (ΔT_d). Orville and Hubbard (1973) have illustrated the relative influence of the first and second terms in Eq. 10. However, their input atmospheric conditions are sufficiently different from those at the seeding level in the Midwest to warrant a more specific calculation for the updrafts under consideration here. Hence, Fig. 13 shows net warming (ΔT), the influence of warming due to latent heat release (ΔT_f), and temperature change related to sublimation/deposition (ΔT_d) for T = -10°C, P = 500 mb. The shaded region in Fig. 13 indicates the range of liquid water contents where both terms in Eq. 10 make a positive contribution to parcel warming. Even though values of net warming are positive over the entire range of liquid water contents, sublimational cooling increasingly negates warming by latent heat release as values of liquid water content increase beyond about 2 g m^{-3}.

Figure 13 also indicates that depositional warming from seeding may be just as important as warming from latent heat released in this sample of Midwestern clouds since liquid water contents tend

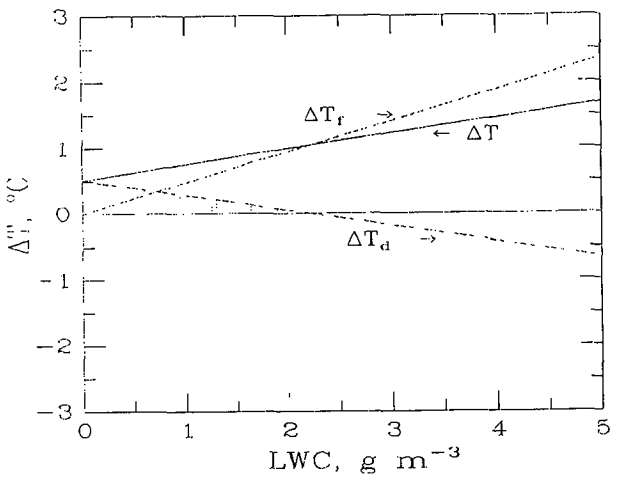

Figure 13. Net and component parcel temperature changes from instantaneous isobaric freezing as a function of liquid water content.

to be low. As illustrated in Fig. 13, the contribution from ΔT_d is greater than that from ΔT_f for liquid water up to about 0.75 g m^{-3}. Hence, seeded clouds with total liquid waters less than 0.75 g m^{-3} may respond positively to seeding, but not directly from warming by latent heat release. Thus the dominance of ΔT_d or ΔT_f may prove to be an important consideration in designating seeding suitability criteria.

Potential buoyancy enhancements (PBE) are shown in Fig. 14 as a function of mean updraft velocity for each updraft for which there was a complete measurement of liquid and solid content in this sample. The solid circles in Fig. 14 show observed buoyancy, including condensate loading, and the open circles show potential buoyancy based on instantaneous isobaric freezing. Computed buoyancy enhancements for young-cloud updrafts averaged 0.64°C (with sample standard deviation $\sigma \approx .2$) and ranged from about one-half to one degree Celsius. Averages for ΔT_f and ΔT_d are 0.26 and 0.38°C, respectively. Hence, over the range of liquid water contents estimated for the updrafts of 1986 clouds, had seeding occurred, the theoretical warming contribution from ΔT_f would have been slightly less than the contribution from ΔT_d (41% compared to

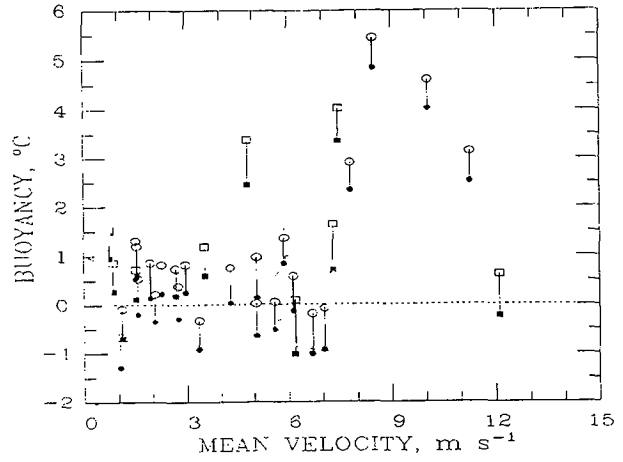

Figure 14. Buoyancy enhancements according to instantaneous isobaric freezing.

61%). Hence, owing to the low total liquid water estimated for this sample, ΔT_d is suggested to be slightly more important than the heat from freezing itself.

Part of the reason that discerning dynamic seeding effects on initial cloud reactions is so difficult can also be inferred from the disposition of the variability in Fig. 14. In the sample, 16 natural updrafts were computed to be negatively buoyant, with the remaining updrafts computed as neutral to positively buoyant. Of the 16 negatively buoyant updrafts, the theory of instantaneous isobaric freezing suggests that 9 would have become neutrally to positively buoyant as a result of seeding. Hence, even within the confines of this small sample, it is suggested that the similar responses to dynamic seeding can not be expected. As can be inferred from Fig. 14, some updrafts may respond to seeding by a decrease in deceleration but still remain in a state of deceleration. Other updrafts may experience a reversal from deceleration to acceleration, and still others may experience an increase in acceleration, all depending on the conditions at the time of seeding. Therefore it is suggested that the practice of discerning seeding effects by using in-cloud measurements must take into account initial buoyancy and potential buoyancy enhancement as covariates to cloud response.

6. SUMMARY AND CONCLUSIONS

PACE86 updrafts at -10°C had the character of air parcels that were experiencing an active coalescence process in the presence of accretional ice processes. The clouds in this small sample contained substantial amounts of supercooled rain, and ice that probably initiated with the freezing of large drops followed by graupel growth by riming. Hence, evolution of natural precipitation in this sample of clouds can be viewed as an orderly transition from an active coalescence process involving supercooled drops to a process of graupel growth by riming, with growth rate advantages (Johnson, 1987). Supercooled water in the form of cloud, drizzle, and raindrops represented an untapped reservoir of latent heat which potentially exists for cloud invigoration by glaciogenic seeding. Therefore, this sample of clouds exhibited many of the ingredients necessary for "dynamic" seeding. However, discerning a seeding response will be complicated by wide variations in cloud conditions at the time of seeding and by differences in the degree of seeding reaction. Tentative key findings about the updrafts in this sample are:

(a) Supercooled Cloud Droplets - Concentrations of these were on the order of 100 to 300 cm^{-3} and liquid water content was low (around 0.3 to 0.4 g m^{-3}). Typically, the effect of entrainment is evident in the structure of the droplet spectra over some cloud transects.

(b) Supercooled Drizzle and Raindrops - The presence of millimeter-size drops in the 2D records gives a clear indication that rapid broadening of the size spectrum occurred by coalescence before the air parcel reached the observation level. The mass of supercooled raindrops typically equalled or exceeded that in the cloud droplets. Thus, FSSP or hot-wire estimates of water content are insufficient

for characterizing seeding suitability. Instead, total liquid water content should be used.

(c) Ice - Graupel occurred in concentrations in excess of that which can be expected from conventional concentrations of ice nuclei. The presence of millimeter size graupel coupled with the time available for riming growth suggest ice initiation by the freezing of millimeter-size raindrops is consistent with the coalesence-freezing precipitation mechanism proposed by Braham (1986). The role of secondary processes such as rime-splintering is still unclear. Typically, the supercooled cloud droplet spectrum met the criteria for riming-splintering. However, direct evidence for rime-splintering could not be established. It appears that entrainment may not necessarily be detrimental to the development of a droplet spectrum which is favorable to rime-splintering. The onset of ice is rapid but not so rapid to initially overwhelm the supply of supercooled drops and subvert seeding opportunity.

(d) Buoyancy and Net Condensate Loading - Natural cloud buoyancies typically clustered around neutral buoyancy, but some were very positive and others were very negative. Loading by the condensate (ice and water) is substantial and has a strong influence in determining net parcel buoyancy.

(e) Buoyancy Enhancement - In the glaciation of midwestern clouds, warming from deposition may be as important as that from the release of latent heat when total liquid water content is around 0.75 g m^{-3}. In the event that no liquid water exists, temperature changes occur solely as a product of deposition. Cloud (updraft) reaction to seeding is sensitively dependent on (i) the velocity of the updraft, (ii) updraft initial buoyancy, and (iii) potential buoyancy enhancement reflected in the initial water and ice content of the updraft. These three factors need to be well accounted for in discerning seeding effects.

7. ACKNOWLEDGEMENTS

The author wishes to thank S. A. Changnon, K. V. Beard, P. C. Kennedy, N. Westcott and the PACE research team for their helpful comments, suggestions and encouragement through the course of this research. Special thanks are owed to Prof. Roscoe R. Braham, Jr. and Dr. Bernice Ackerman for the ideas they stimulated in the analysis. The author also wishes to thank Norm Ostrander (pilot) and Don Stone (flight engineer) for their dedicated efforts in pursuit of these data. Finally, the author wishes to thank several undergraduate students (Lisa Brown, Matt Walters, and Hiten Ranwintwa) for their careful work in classifying and processing the image data. The research was supported under NOAA cooperative agreements COM NA86RA06051, COM NA87RAH07077, COM NA88RAH08107, COM NA89RAH09086 and COM NA90AA-H-0A175.

8. REFERENCES

Ackerman, B.A., R.C. Grosh, and R.Y. Sun, 1978: Assessing Midwest cloud characteristics for weather modification. Illinois State Water Survey, Final Report ENV77-11527, 128 pp.

Ackerman, B.A., and N.E. Westcott, 1986: Midwestern convective clouds: A review. *Jour. of Weather Modification*, **18**, 87-94.

Beard, K.V., 1976: Terminal velocity and shape of cloud and precipitation drops aloft. *J. Atmos. Sci.*, **33**, 851-864.

Berry, E. X, and R.L. Reinhardt, 1974: An analysis of cloud drop growth by collection: Parts I-IV. *J. Atmos. Sci.*, **31**, 1814-1831, 2118-2135.

Braham, R.R., 1964: What is the role of ice in summer rain-showers? *J. Atmos. Sci.*, **21**, 640-645.

Braham, R.R., Jr., 1986: The cloud physics of weather modification. Part I. Scientific basis. WMO Bulletin, **35**, 215-222.

Byers, H.R., and Braham, R.R., Jr., 1949: The thunderstorm: Report of the thunderstorm project. Washington, D.C.: U.S. Government Printing Office.

Cerni, T.A., 1983: Determination of the size and concentration of cloud drops with an FSSP. *J. Climate Appl. Meteor.*, **22**, 1346-1355.

Changnon, S.A., 1986: Illinois weather modification program: PACE. Preprints Conference on Weather Modification, Arlington, Virginia.

Cooper, W.A., 1988: Effects of coincidence on measurements with a forward scattering spectrometer probe. *J. Atmos. and Oceanic Technol.*, **5**, 823-832.

Cornford, S.G., 1967: Sampling errors in measurements of raindrop and cloud droplet concentrations. *Met. Mag., London*, **96**, 271-282.

Dye, J.E., and D. Baumgardner, 1984: Evaluation of the forward scattering spectrometer probe. Part I: Electronic and optical studies. *J. Atmos. Oceanic Technol.*, **1**, 329-344.

Fletcher, N. H., 1962: *Physics of Rain Clouds*. Cambridge University Press, 390 pp.

Fukuta, N., 1973: Thermodynamics of cloud glaciation. *J. Atmos. Sci.*, **30**, 1645-1649.

Gardiner, B.A., and J. Hallett, 1985: Degradation of in-cloud forward scattering spectrometer probe measurements in the presence of ice particles. *J. Atmos. and Oceanic Technol.*, **2**, 171-180.

Hallett, J., R.I. Sax, D. Lamb, and A.S. Ramachandra Murty, 1978: Aircraft measurements of ice in Florida cumuli. *Quart. J. Roy. Meteor. Soc.*, **104**, 631-651.

Hallett, J., and S.C. Mossop, 1974: Production of secondary ice crystals during the riming process. *Nature*, **249**, 26-28.

Harris-Hobbs R.L., and W.A. Cooper, 1987: Field evidence supporting quantitative predictions of secondary ice production rates. *J. Atmos. Sci.*, **44**, 1071-1082.

Heymsfield, A.J., 1978: The characteristics of graupel particles in northeastern Colorado cumulus congestus clouds. *J. Atmos. Sci.*, 35, 284-295.

Heymsfield, A.J., and D. Baumgardner, 1985: Summary of a workshop on processing 2-D probe data. *Bull. Amer. Meteor. Soc.*, 66, 437-440.

Johnson, D.B., 1987: On the relative efficiency of coalescence and riming. *J. Atmos. Sci.*, 44, 1671-1680.

Lawson, R.P., 1979: A system for airborne measurement of vertical air velocity. *J. Appl. Met.*, 18, 1363-1368.

Lenchow, D.H., 1976: Estimating updraft velocity from an airplane response. *Mon. Wea. Rev.*, 104, 618-626.

MacCready, P.F., Jr., and R.R. Skutt, 1967: Cloud buoyancy increase due to seeding. *J. Appl. Met.*, 6, 207-210.

Mossop, S.C., 1978: The influence of drop size distribution on the production of secondary ice particles during graupel growth. *Quart. J. R. Met. Soc.*, 104, 323-330.

Mossop, S.C., 1976: Production of secondary ice particles during the growth of graupel by riming. *Quart. J. Roy. Meteor. Soc.*, 102, 45-57.

Mossop, S.C., and J. Hallett, 1974: Ice crystal concentrations in cumulus clouds: Influence of drop spectrum. *Science*, 186, 632-634.

Orville, H.D., and K. Hubbard, 1973: On the freezing of liquid water in a cloud. *J. Appl. Met.*, 12, 671-676.

Orville, H.D., F.J. Kopp, R.D. Farley, and R.B. Hoffman, 1989: The numerical modeling of ice-phase cloud seeding effects in a warm-based cloud. Preprints, 5th WMO Scientific conference on Weather Modification and Applied Cloud Physics, Beijing, China, 203-207.

Politovich, M.K., and R.F. Reinking, 1987: Characteristics of updrafts in central Illinois cumuli. Preprints, 11th Conference on Weather Modification, Edmonton, Alberta, Canada, 68-71.

Rangno, A. L., and P. V. Hobbs, 1983: Production of ice particles in clouds due to aircraft penetrations. *J. Climate Appl. Meteor.*, 22, 214-232.

Rangno, A. L., and P. V. Hobbs, 1984: Further observations of the production of ice particles in clouds by aircraft. *J. Climate Appl. Meteor.*, 23, 985-987.

Saunders, P.M., 1957: The thermodynamics of saturated air: A contribution to classical theory. *Quart. J. Roy. Meteor. Soc.*, 83, 342-350.

Scott, B.C., and P.V. Hobbs, 1977: A theoretical study of the evolution of mixed-phased cumulus clouds. *J. Atmos. Sci.*, 34, 812-826.

Simpson, J., and A.S. Dennis, 1974: Cumulus clouds and their modification. *Weather and Climate Modification*, W.N. Hess editor, John Wiley and Sons, New York, 842 pp.

Spyers-Duran, P.A., 1968: Comparative measurements of cloud liquid water using heated wire and cloud replicating devices. *J. Appl. Met.*, 7, 674-678.

Strapp, J.W., and R.S. Schemenauer, 1982: Calibrations of the Johnson Williams liquid water content meters in a high-speed icing tunnel. *J. Appl. Met.*, 21, 98-108.

Warner, J., 1969: The microstructure of cumulus clouds. Part I. General features of the droplet spectrum. *J. Atmos. Sci.*, 26, 1049-1059.

Woodley, W.L., 1970: Rainfall enhancement by dynamic cloud modification. *Science*, 170, 127-131.